



Cycle 30 - Cycle 32 COS NUV Spectroscopic Sensitivity Monitor

Jacqueline Hernandez¹

¹ Space Telescope Science Institute, Baltimore, MD

16 December 2025

ABSTRACT

Observations of HST spectrophotometric standard stars show that the COS NUV detector has a time-dependent sensitivity (TDS) that must be monitored and accounted for in flux calibration. Regular observations monitor the changes in sensitivity for three NUV gratings: G230L, G185M, and G225M. The fourth NUV grating, G285M, was removed from routine monitoring because its sensitivity has become too low. G285M continues to be available but unsupported for General Observer programs. In this ISR, I present the results of the Cycle 30, Cycle 31, and Cycle 32 NUV TDS programs.

Contents

1. Introduction	2
2. Observations	2
2.1 Cycle 30	2
2.2 Cycle 31	3
2.3 Cycle 32	3
3. Analysis and Results	4
3.1 Cycle 30	4
3.2 Cycle 31	4
3.3 Cycle 32	7
4. Continuation Plan	8
Change History for COS ISR 2025-20	8
References	8

1. Introduction

The near-ultraviolet (NUV) channel onboard the Cosmic Origins Spectrograph (COS) uses a Multi-Anode Microchannel Array (MAMA) detector. This channel can be used with a series of gratings, three medium resolution gratings (G185M, G225M, and G285M) and one low resolution grating (G230L). A given grating projects one spectral trace to three detector stripes (NUVA, NUVB, NUVC), which simultaneously cover three different wavelength ranges. The detector is also sensitive to second-order contamination (see Section 5.1.3 of the COS instrument Handbook; Fischer 2025).

Loss in sensitivity as a function of time was noted in the G225M and G285M gratings shortly before the launch of COS in 2009. An oxide layer formed over the bare aluminum G225M and G285M gratings and caused the sensitivity to decline over time (Osten et al. 2010). The G185M and G230L gratings remained stable due to a MgF_2 coating that prevented the formation of an oxide layer. Regular observations of spectrophotometric standard stars were established to monitor for the time dependent sensitivity (TDS) and account for in flux calibration (Osten et al. 2010). The COS NUV TDS program executes every cycle and monitors the sensitivity of the NUV gratings, except for G285M as it has lost over 85% of its original sensitivity since launch and now continues to be unsupported but available for general users (Fischer 2019). These changes are characterized as functions of grating and wavelength. The results of this program are used to update the COS NUV TDS reference file, TDSTAB, as well as synphot files that are used as inputs for the exposure time calculator.

In this ISR, I review the results from the Cycle 30, Cycle 31, and Cycle 32 NUV TDS programs.

2. Observations

2.1 Cycle 30

The Cycle 30 NUV TDS program (16937, PI W. Fischer) was designed with two pairs of visits. The first pair, a one-orbit visit for the L grating (L1) and a one-orbit visit for the M gratings (M1) ran on 2023 February 20 and 23, respectively. Visit L1 observed the white dwarf standard WD1057+719 with grating G230L (central wavelengths (cenwaves) 2635 and 2950). Visit M1 observed the white dwarf standard G191-B2B with gratings G185M (cenwaves 1786, 1921, and 2010) and G225M (cenwaves 2186, 2306, and 2410). The second pair of visits, L2 and M2, were identical to the first and ran on 2023 August 20. All four visits executed successfully.

For all visits, the acquisition consisted of the sequence ACQ/SEARCH, ACQ/PEAKXD, and ACQ/PEAKD. Cenwave 2010 was used for the M visits and cenwave 2635 was used for the L visits. All data were obtained at the default FP-POS 3 because the fixed-pattern noise when a single FP-POS is used in the NUV limits the signal-to-noise ratio to 50 per resolution element, in excess of what is needed to characterize TDS to better than 5%.

The program was identical to its Cycle 29 predecessor (16537, PI W. Fischer). This and previous ISRs on this topic (e.g., Fischer 2023) show that the TDS of G225M is $-3\% \text{yr}^{-1}$, while the TDS of other supported gratings is close to 0.

2.2 Cycle 31

The Cycle 31 NUV TDS program (17319, PI J. Hernandez) was designed with two pairs of visits, identical to its Cycle 30 predecessor in Section 2.1. The exposure and buffer times were updated for the G225M exposures, increased on average by 6.05% and 9.38%, respectively, to account for the declining sensitivity.

The first pair of visits, L1 and M1, ran on 2024 March 9 and 10. The second pair of visits, M2 and L2, ran on 2024 September 5 and 19. All four visits executed successfully.

2.3 Cycle 32

The Cycle 32 NUV TDS program (17618, PI J. Hernandez) was designed with two pairs of visits. Unlike its Cycle 31 predecessor in Section 2.2, the M visits were modified to remove the cenwave G225M/2306 and replace with cenwave G225M/2233. This is to increase the wavelength range monitored and support the wavelength dependent TDSTAB available for users. Archival data of white dwarf standard GD71 were used to provide a long-term view of the TDS of this new wavelength and scaled for future G191-B2B observations (Hernandez et al. 2025).

The first pair of visits, L1 and M1, ran on 2025 March 30 and April 2, respectively. The second pair of visits, L2 and M2, both ran on 2025 September 28. Three of the four visits executed successfully. For visit L1, the Fine Guidance Sensors lost lock on the guide stars before the COS acquisition began and thus the shutter was closed for a majority of the visit. Visit L1 was repeated as visit L3 and ran successfully on 2025 May 19.

For all visits, the acquisition consisted of the sequence ACQ/PEAKXD and ACQ/PEAKD. The initial ACQ/SEARCH was removed due to redundancy as the coordinates of both targets, WD1057+719 and G191-B2B, are well documented.

The exposure and buffer times were updated for the G225M exposures. Exposure times were increased on average by 7.55% and buffer times were increased on average by 3.66% to account for the declining sensitivity. The exposures times were updated for the G185M exposures, as well. Exposure times were decreased on average by 2.71%, accounting for the increasing sensitivity.

3. Analysis and Results

The computation of the TDS for COS NUV data is described in previous ISRs (Osten et al. 2010; 2011). For each cenwave and stripe, we calculate the ratio of every net-counts spectrum to the first obtained (the first observations were in 2009 August for G230L and G225M/2233, 2009 September for G225M/2186-2306-2410 and G185M/1921, 2011 November for G185M/1786, and 2017 January for G185M/2010). The ratio as a function of wavelength is condensed to a single value by averaging over the full stripe. The relationship of ratio to observation date obtained for each stripe is then fit with a straight line. Here we report the slopes of the lines when the ratios are taken to be 1 at the time each cenwave was first monitored. In the TDSTAB, since a uniform reference date is required, rescaling the ratios to unity in the reference date results in slightly different values from those presented here.

3.1 Cycle 30

For each grating, the spread in slopes among the monitored cenwaves and stripes is generally small, so here we report the slopes of each cenwave/stripe combination in Table 1. Figures 1 through 8 show the linear fits for each observed cenwave. G230L and G185M gratings are coated in MgF_2 , mean and standard deviation of the slopes are consistent with no change ($0.03 \pm 0.21 \text{ \% yr}^{-1}$) and a mild increase in sensitivity ($0.08 \pm 0.11 \text{ \% yr}^{-1}$), respectively. However, by the individual slope values of each cenwave/stripe combination, there appears to be a new feature beginning at the start of 2022. This feature increases the sensitivity of the shortest wavelengths of G185M and G230L (G185M/1786/NUVA and G230L/2635/NUVA) while the rest of the gratings show decreases in sensitivity. This feature is not visible in G225M, a grating of bare aluminum. G225M continues to show significant decline in sensitivity ($-2.86 \pm 0.14 \text{ \% yr}^{-1}$).

3.2 Cycle 31

We report the slopes of each cenwave/stripe combination in Table 2 and the mean and standard deviation here. Figures 9 through 16 show the linear fits for each observed cenwave. G230L and G185M are consistent with no change ($0.03 \pm 0.21 \text{ yr}^{-1}$ and $-0.01 \pm 0.21 \text{ yr}^{-1}$, respectively). As reported in Section 3.2, there appears to be a feature beginning at the start of 2022 for each individual cenwave/stripe combination. The sensitivity continues to increase for the shortest wavelengths of G185M and G230L (G185M/1786/NUVA and G230L/2635/NUVA) while the rest of the gratings decrease in sensitivity. This feature is not visible in G225M and the grating continues to show significant decline in sensitivity ($-2.88 \pm 0.14 \text{ yr}^{-1}$).

Table 1. Cycle 30 NUV TDS Program 16937 Results

COS Grating	Cenwave	Stripe	Slope ($\% yr^{-1}$)
G230L	2635	NUVA	0.45
		NUVB	-0.08
		NUVC	-0.02
	2950	NUVA	0.13
		NUVB	-0.13
		NUVC	-0.16
G185M	1786	NUVA	0.32
		NUVB	0.22
		NUVC	0.11
	1921	NUVA	0.19
		NUVB	0.09
		NUVC	-0.02
	2010	NUVA	-0.01
		NUVB	-0.10
		NUVC	-0.04
G225M	2186	NUVA	-2.45
		NUVB	-2.95
		NUVC	-3.00
	2306	NUVA	-2.95
		NUVB	-2.97
		NUVC	-2.89
	2410	NUVA	-2.92
		NUVB	-2.83
		NUVC	-2.80

Table 2. Cycle 31 NUV TDS Program 17319 Results

COS Grating	Cenwave	Stripe	Slope ($\% yr^{-1}$)
G230L	2635	NUVA	0.43
		NUVB	-0.09
		NUVC	-0.09
	2950	NUVA	0.08
		NUVB	-0.13
		NUVC	-0.20
G185M	1786	NUVA	0.35
		NUVB	0.20
		NUVC	0.03
	1921	NUVA	0.16
		NUVB	0.02
		NUVC	-0.08
	2010	NUVA	-0.24
		NUVB	-0.36
		NUVC	-0.17
G225M	2186	NUVA	-2.50
		NUVB	-2.96
		NUVC	-3.01
	2306	NUVA	-2.98
		NUVB	-2.99
		NUVC	-2.91
	2410	NUVA	-2.93
		NUVB	-2.84
		NUVC	-2.81

Table 3. Cycle 32 NUV TDS Program 17618 Results

COS Grating	Cenwave	Stripe	Slope ($\% \text{ yr}^{-1}$)
G230L	2635	NUVA	0.41
		NUVB	-0.09
		NUVC	-0.14
	2950	NUVA	0.03
		NUVB	-0.13
		NUVC	-0.24
G185M	1786	NUVA	0.34
		NUVB	0.18
		NUVC	-0.04
	1921	NUVA	0.12
		NUVB	-0.04
		NUVC	-0.13
	2010	NUVA	-0.38
		NUVB	-0.49
		NUVC	-0.22
G225M	2186	NUVA	-2.56
		NUVB	-2.99
		NUVC	-3.03
	2233 ^a	NUVA	-2.85
		NUVB	-3.06
		NUVC	-3.03
	2410	NUVA	-2.95
		NUVB	-2.86
		NUVC	-2.83

^aG225M/2306 was replaced by G225M/2233 at the start of Cycle 32.

3.3 Cycle 32

We report the slopes of each cenwave/stripe combination in Table 3 and the mean and standard deviation here. Figures 17 through 24 shows the linear fits for each observed cenwave. G230L and G185M are consistent with a decline in sensitivity ($-0.16 \pm 0.21 \text{ yr}^{-1}$ and $-0.66 \pm 0.25 \text{ yr}^{-1}$, respectively). As reported in Section 3.1, there continues to be a featuring beginning at the start of 2022 for each individual cenwave/stripe combination. The sensitivity continues to increase for the shortest wavelengths of G185M and G230L (G185M/1786/NUVA and G230L/2635/NUVA) while the rest of the gratings decrease in sensitivity. This feature is not visible in G225M, which continues to show significant decline ($-2.91 \pm 0.14 \text{ yr}^{-1}$).

4. Continuation Plan

This program continues in Cycle 33 as PID 17936 and is identical to the Cycle 32 version. Instrument documentation reflects the available but unsupported status of the G285M grating. Users who are interested in spectroscopic coverage of the wavelength range from 2500 to 3200 Å at the G285M resolution are encouraged to use the G230M or E230M gratings on the Space Telescope Imaging Spectrograph (STIS) instead.

Change History for COS ISR 2025-20

Version 1: 16 December 2025- Original Document

References

- Fischer, W. J. 2019, COS Instrument Science Report 2019-12
Fischer, W. J., 2023, COS Instrument Science Report 2023-27
Hernandez, J. et al, 2025, COS Instrument Science Report 2025-16
Osten, R. A., et al. 2010, COS Instrument Science Report 2010-15
Osten, R. A., et al. 2011, COS Instrument Science Report 2011-02

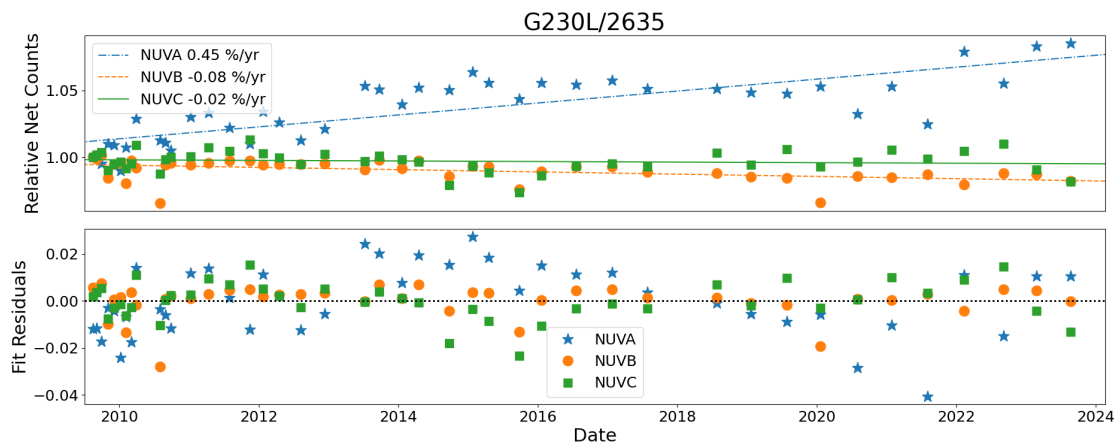


Figure 1. NUV TDS results for the G230L/2635 setting from the Cycle 30 program, with blue for stripe NUVA, orange for stripe NUVB, and green for stripe NUVC. Top: Relative sensitivity versus time, where the first measurement for each stripe is scaled to 1. The linear fits are shown; they cross at a time that depends on the details of each fit. The slopes are given in the legend. Bottom: Residuals from the linear fits.

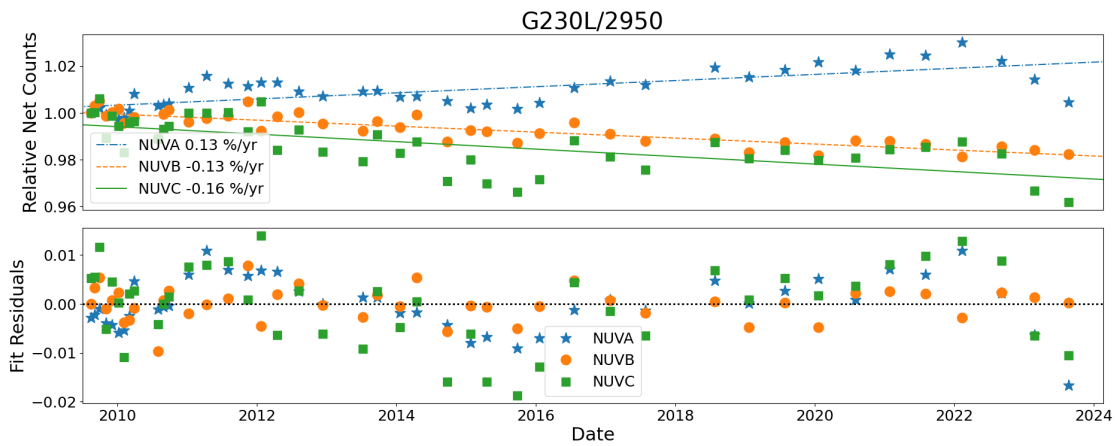


Figure 2. Results for Cycle 30 G230L/2950. See the caption to Figure 1 for details.

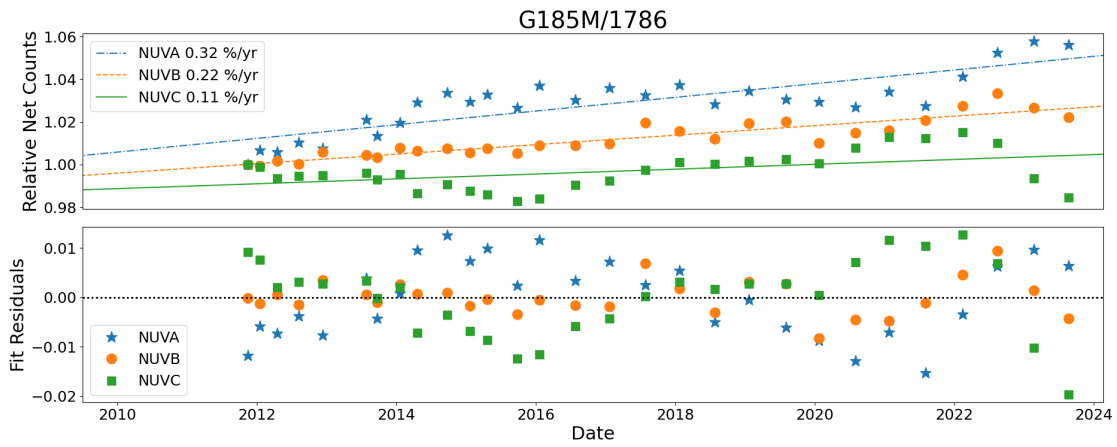


Figure 3. Results for Cycle 30 G185M/1786. See the caption to Figure 1 for details.

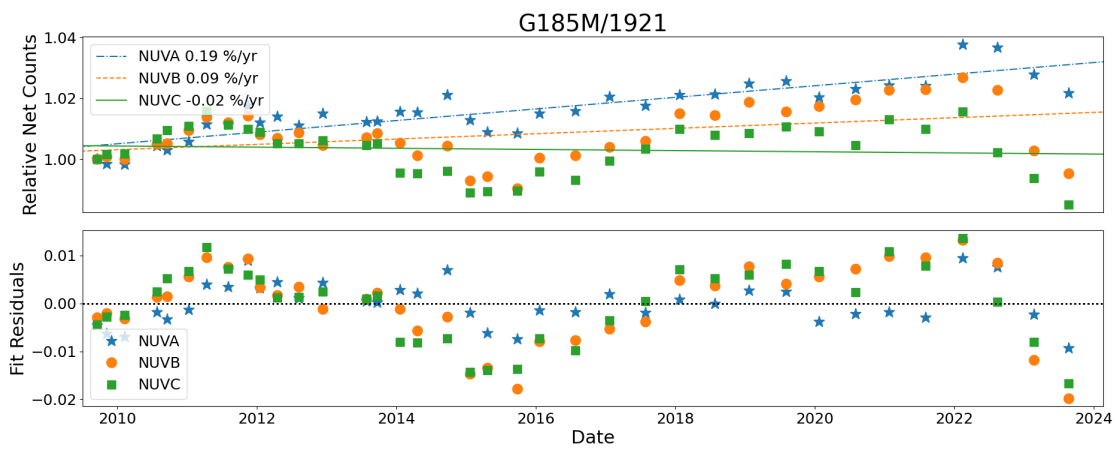


Figure 4. Results for Cycle 30 G185M/1921. See the caption to Figure 1 for details.

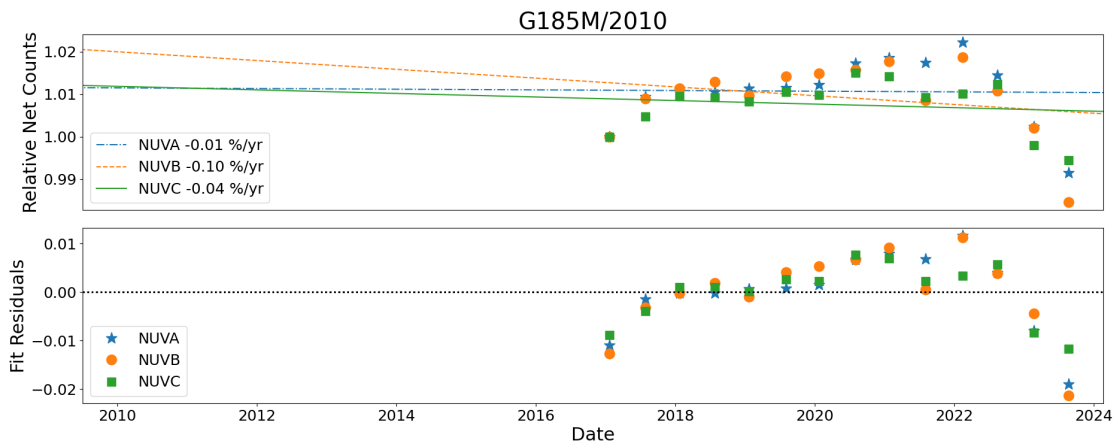


Figure 5. Results for Cycle 30 G185M/2010. See the caption to Figure 1 for details.

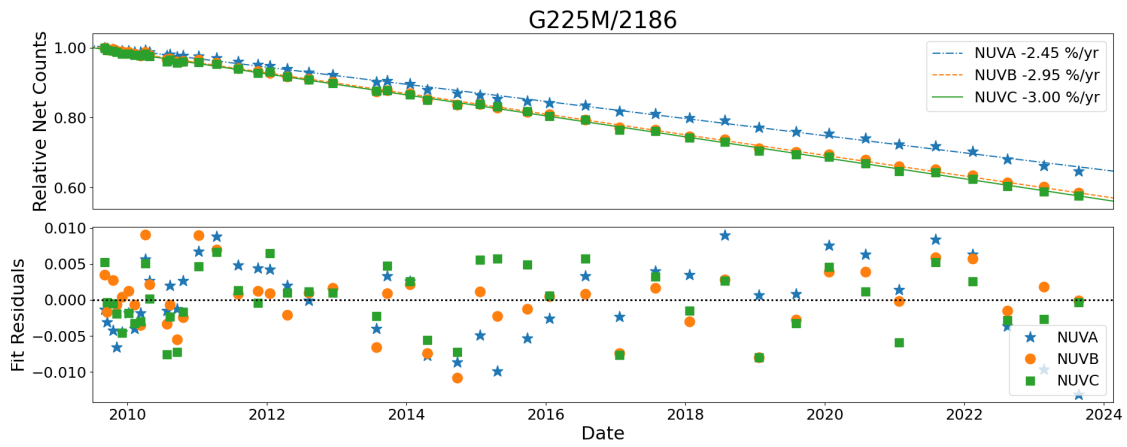


Figure 6. Results for Cycle 30 G225M/2186. See the caption to Figure 1 for details.

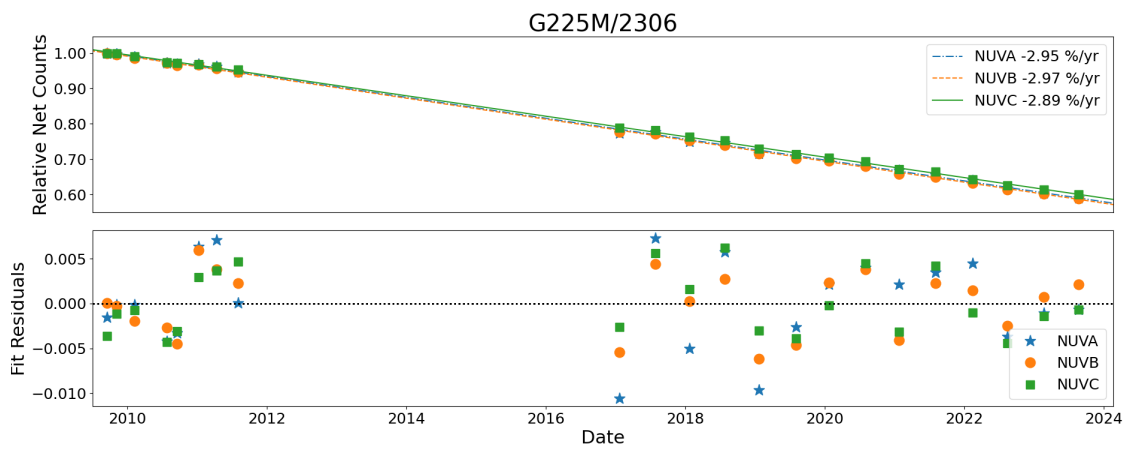


Figure 7. Results for Cycle 30 G225M/2306. See the caption to Figure 1 for details.

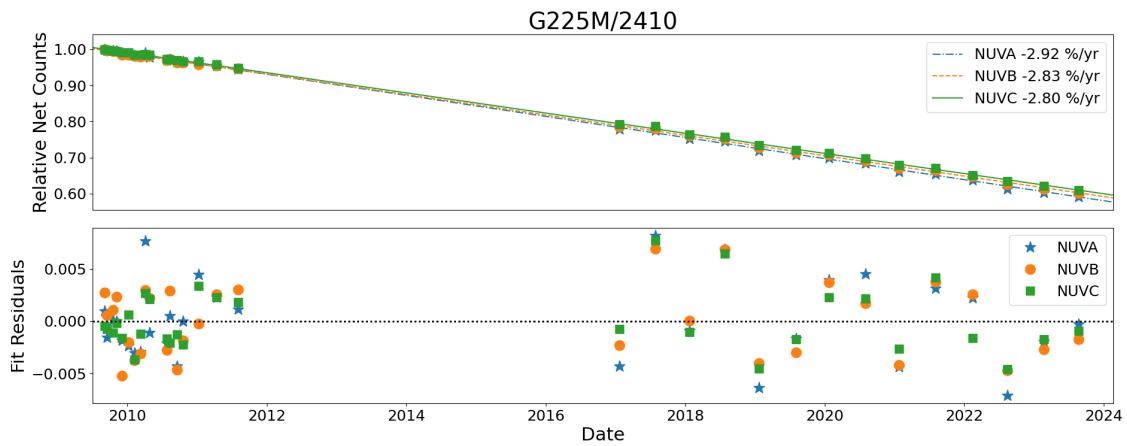


Figure 8. Results for Cycle 30 G225M/2410. See the caption to Figure 1 for details.

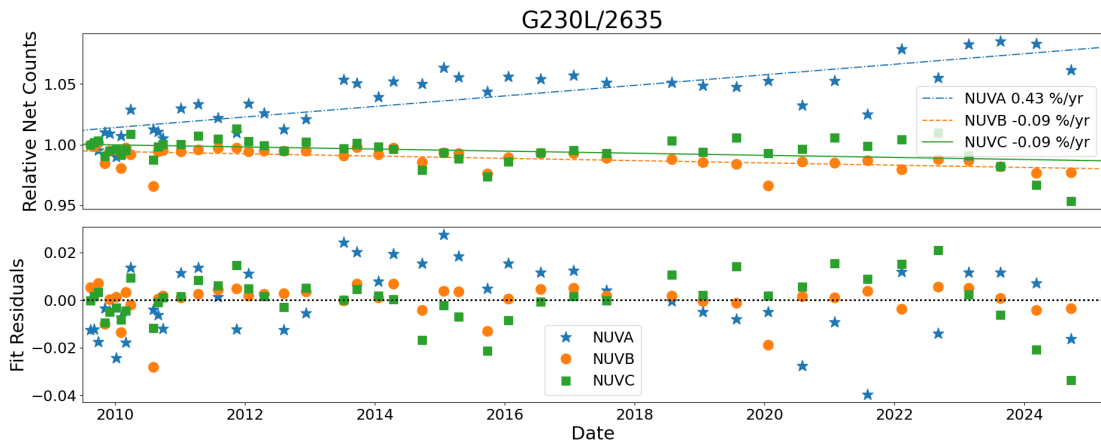


Figure 9. Results for Cycle 31 G230L/2635. See the caption to Figure 1 for details.

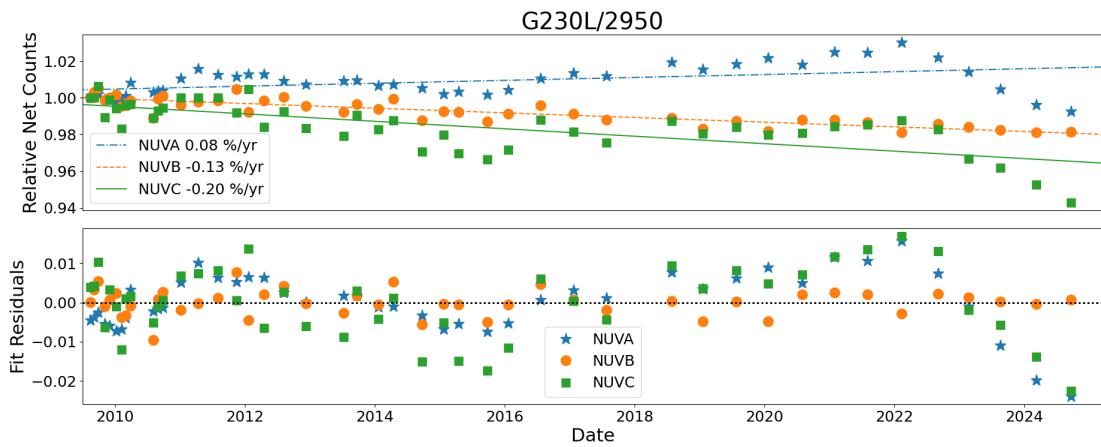


Figure 10. Results for Cycle 31 G230L/2950. See the caption to Figure 1 for details.

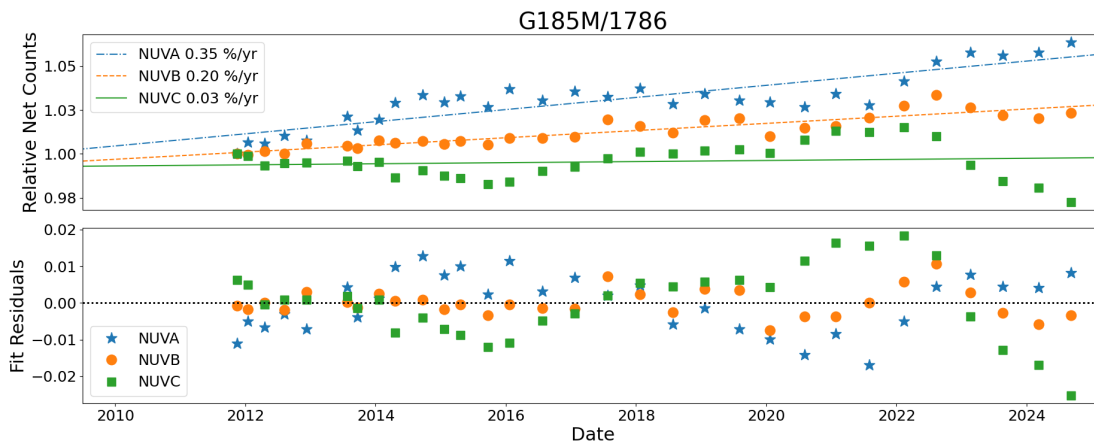


Figure 11. Results for Cycle 31 G185M/1786. See the caption to Figure 1 for details.

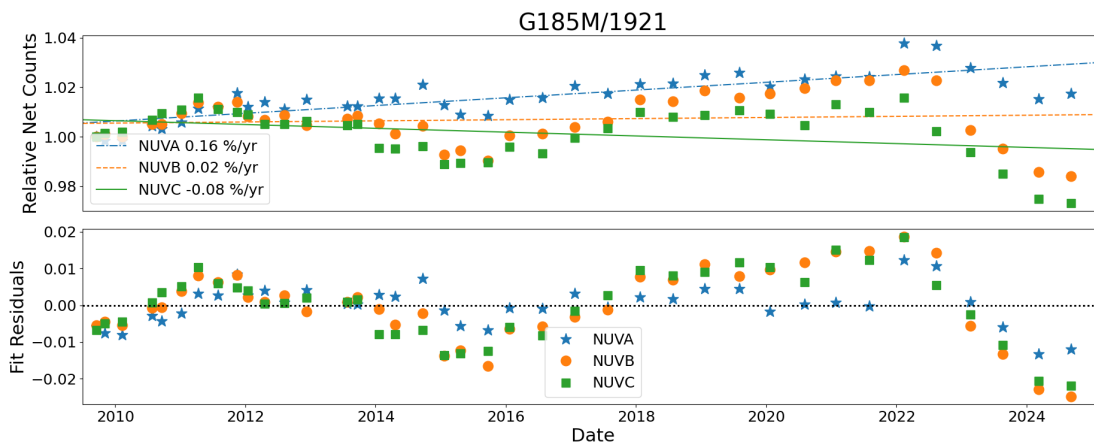


Figure 12. Results for Cycle 31 G185M/1921. See the caption to Figure 1 for details.

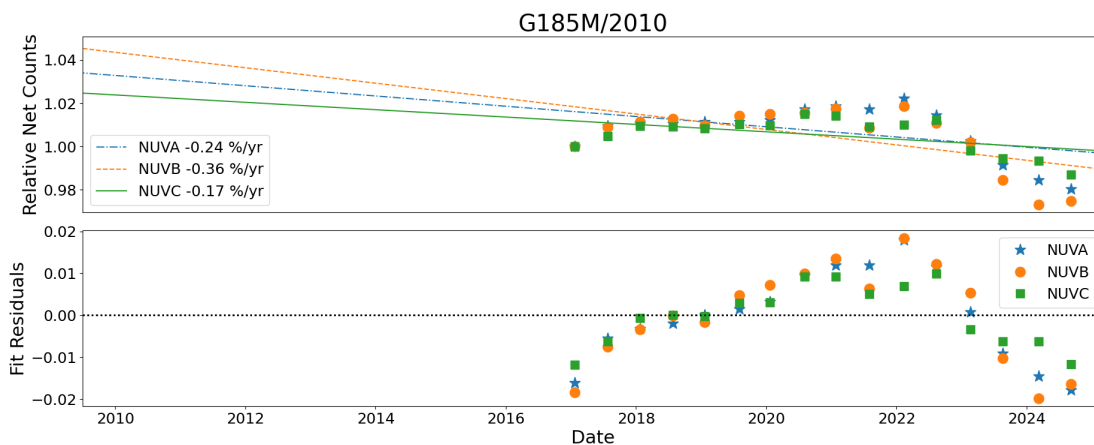


Figure 13. Results for Cycle 31 G185M/2010. See the caption to Figure 1 for details.

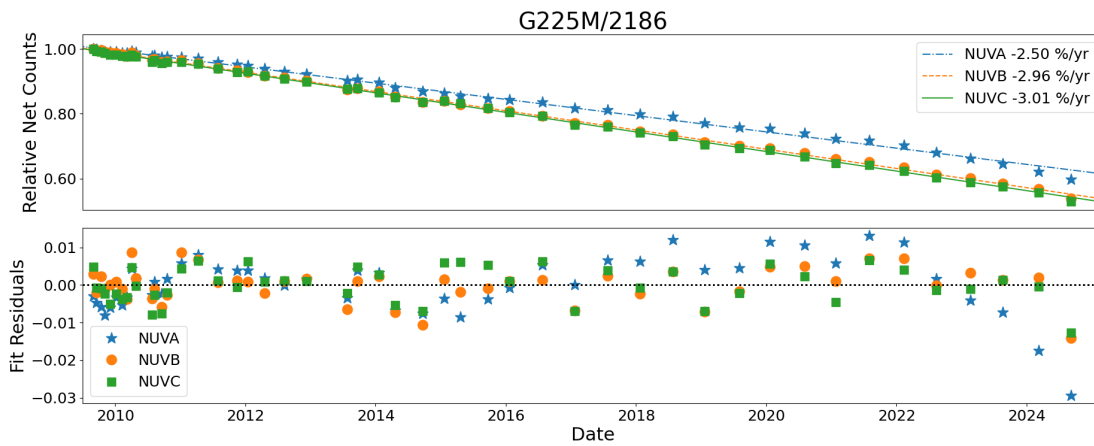


Figure 14. Results for Cycle 31 G225M/2186. See the caption to Figure 1 for details.

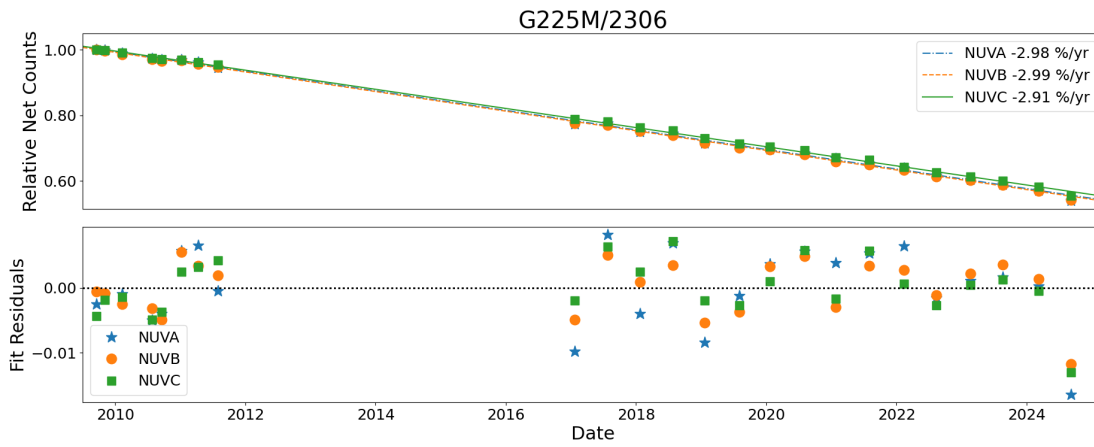


Figure 15. Results for Cycle 31 G225M/2306. See the caption to Figure 1 for details.

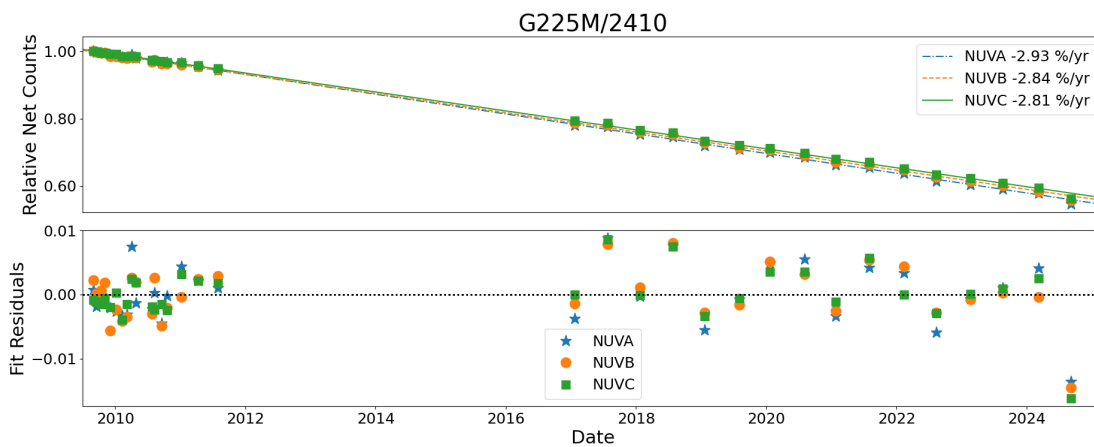


Figure 16. Results for Cycle 31 G225M/2410. See the caption to Figure 1 for details.

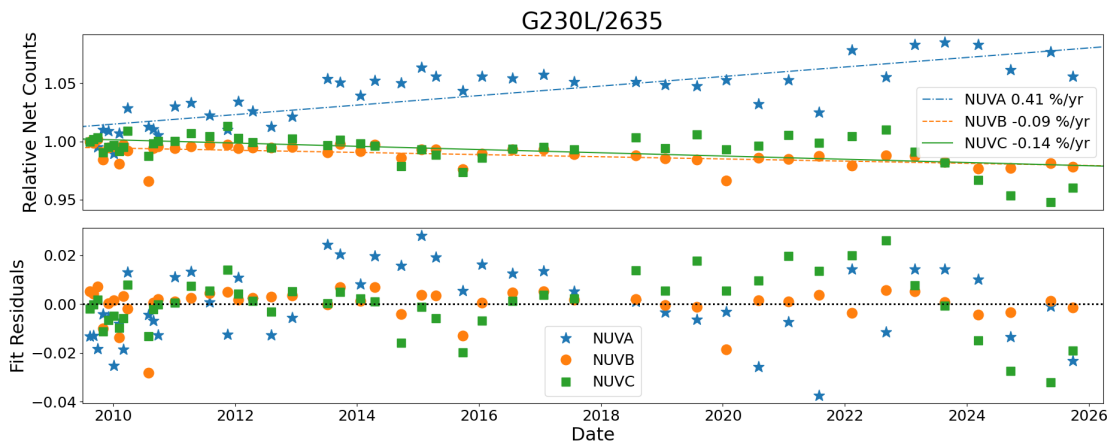


Figure 17. Results for Cycle 32 G230L/2635. See the caption to Figure 1 for details.

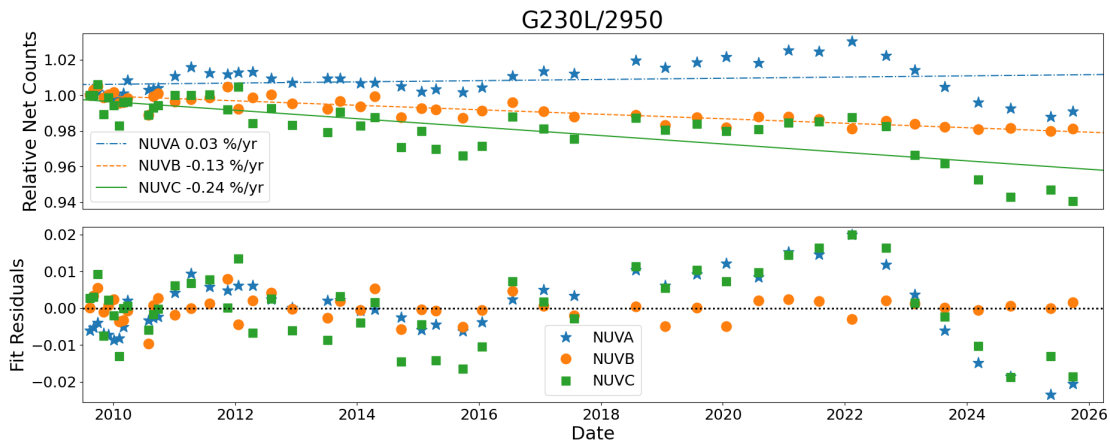


Figure 18. Results for Cycle 32 G230L/2950. See the caption to Figure 1 for details.

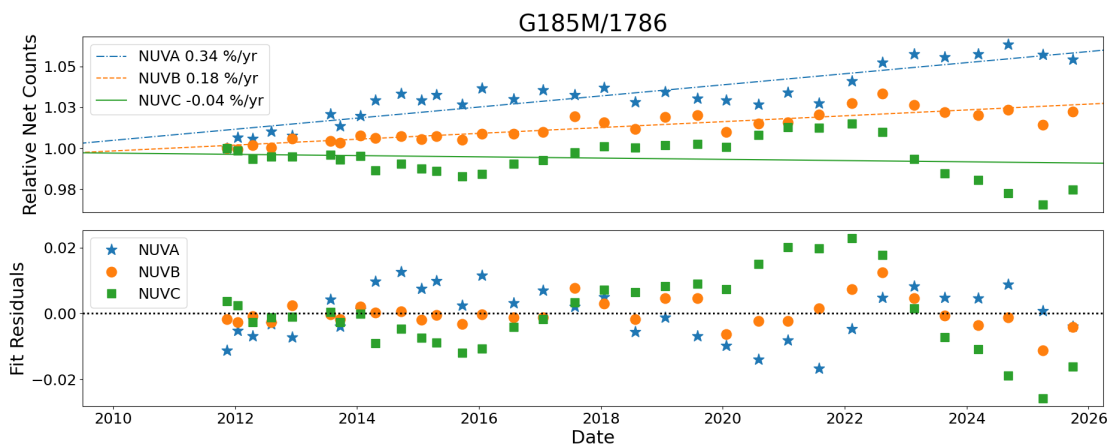


Figure 19. Results for Cycle 32 G185M/1786. See the caption to Figure 1 for details.

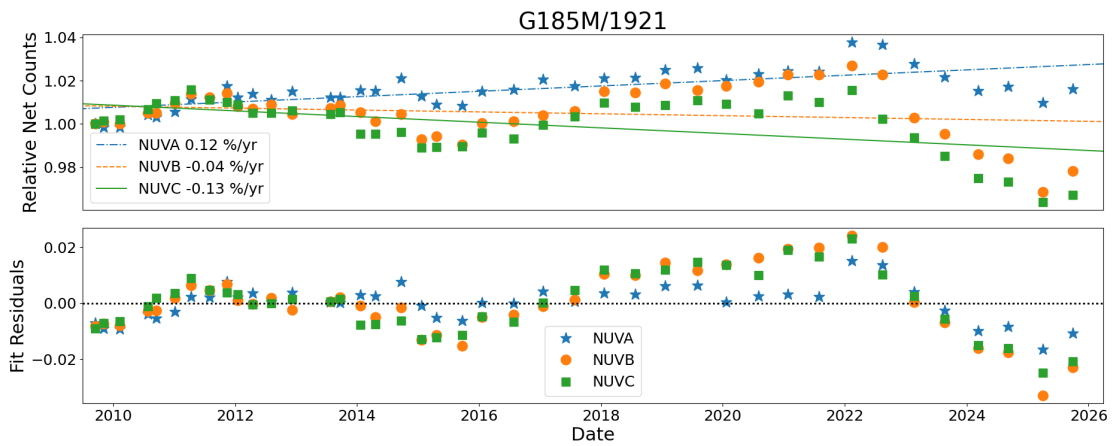


Figure 20. Results for Cycle 32 G185M/1921. See the caption to Figure 1 for details.

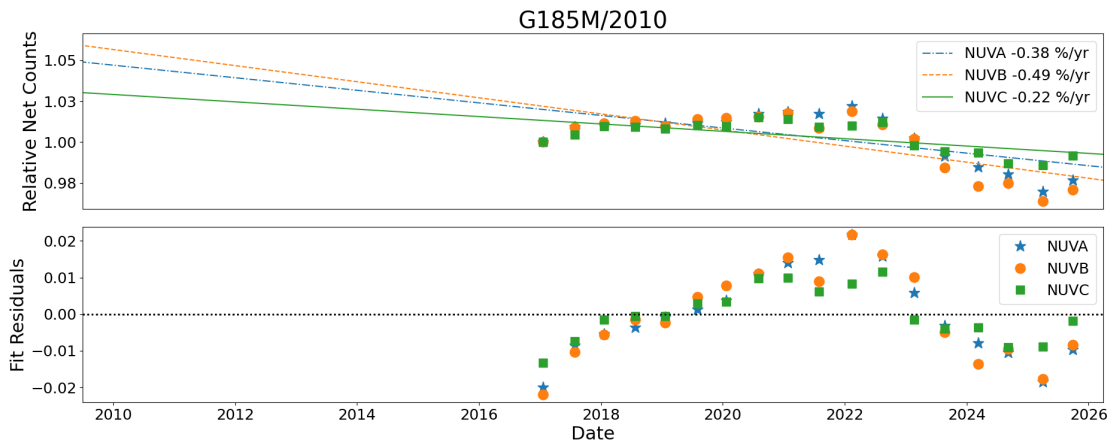


Figure 21. Results for Cycle 32 G185M/2010. See the caption to Figure 1 for details.

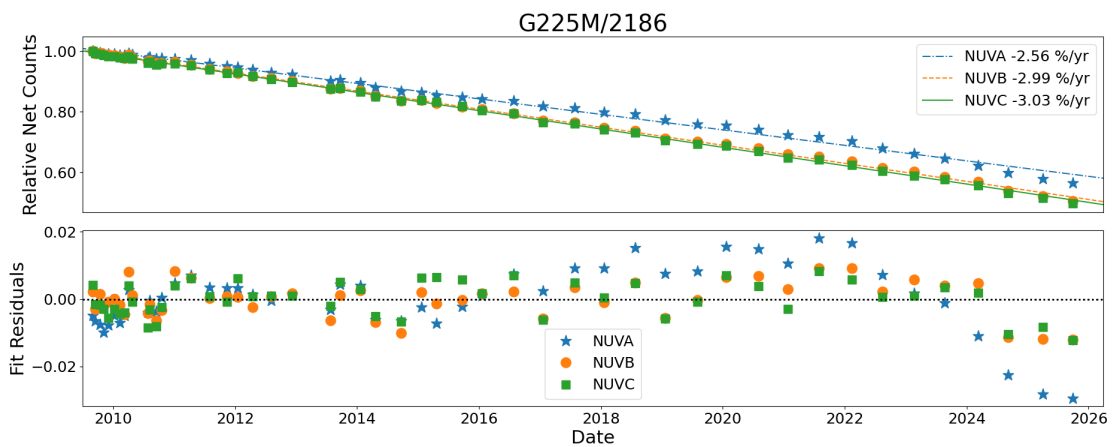


Figure 22. Results for Cycle 32 G225M/2186. See the caption to Figure 1 for details.

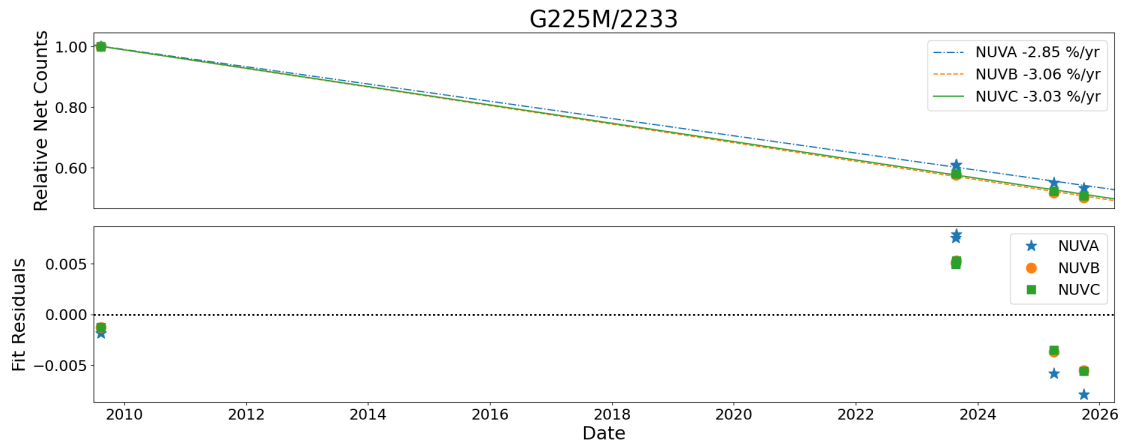


Figure 23. Results for Cycle 32 G225M/2233. See the caption to Figure 1 for details.

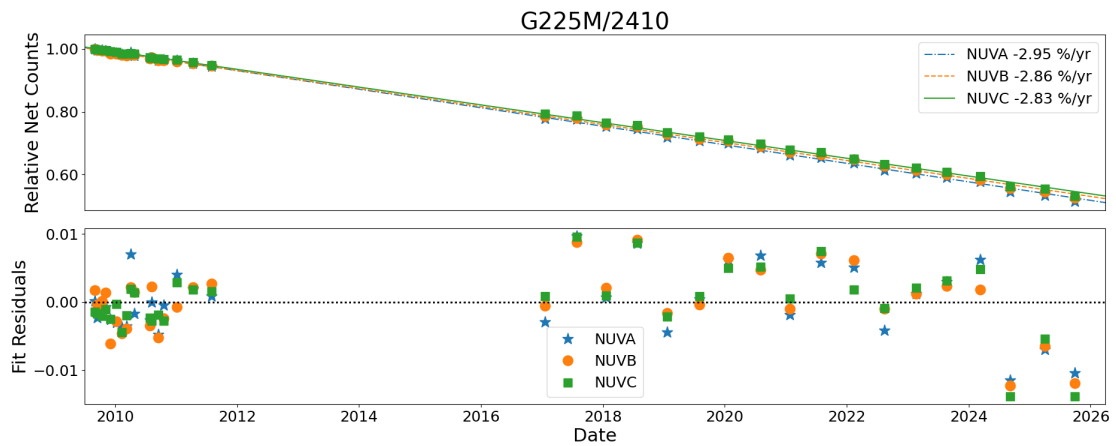


Figure 24. Results for Cycle 32 G225M/2410. See the caption to Figure 1 for details.